J Fluoresc (2009) 19:311–316
DOI 10.1007/s10895-008-0417-z

ORIGINAL PAPER

Self-assembly Drives Quantum Dot Photoluminescence

J. Plain · Y. Sonnefraud · P. Viste · G. Lérondel · S. Huant · P. Royer

Received: 4 April 2008 / Accepted: 3 September 2008 / Published online: 16 September 2008

Abstract Engineering the spectral properties of quantum dots can be achieved by a control of the quantum dots organization on a substrate. Indeed, many applications of quantum dots as LEDs are based on the realization of a 3D architecture of quantum dots. In this contribution, we present a systematic study of the quantum dot organization obtained on different chemically modified substrates. By varying the chemical affinity between the quantum dots and the substrate, the quantum dot organization is strongly modified from the 2D monolayer to the 3D aggregates. Then the photoluminescence of the different obtained samples has been systematically studied and correlated with the quantum dot film organization. We clearly show that the interaction between the substrate and the quantum dot must be stronger than the quantum dot–quantum dot interaction to avoid 3D aggregation and that these organization strongly modified the photoluminescence of the film rather than intrinsic changes of the quantum dot induced by pure surface chemistry.

Keywords Self assembly · Quantum dot · Photoluminescence

J. Plain (✉) · P. Viste · G. Lérondel · P. Royer
Laboratoire de Nanotechnologie et d'Instrumentation Optique,
LRC CEA/LETI, ICD FRE CNRS 2848,
Université de Technologie de Troyes,
12 rue Marie Curie, BP2060, 10010 Troyes cedex, France
e-mail: jerome.plain@utt.fr

Y. Sonnefraud · S. Huant
Institut Néel, CNRS and Université Joseph Fourier,
25 avenue des Martyrs, BP 166, 38042 Grenoble cedex 9, France

Introduction

Colloidal semiconductor quantum dots (QDs) are widely used for new optical applications as white light emitting diodes [1], solar cells [2, 3], or biological and chemical labels [4–6]. Their wide size-tuneable emission energy, high photostability, narrow emission linewidths, very good photoluminescence quantum efficiency make them very good candidates to be used as optically active part in devices [7]. In particular, a very important issue is to address the semiconductor nanoparticles as ultrathin films without loss of their promising optical properties. Then, numerous studies have been dedicated to the possibility of organizing the nanoparticles in thin films [8–10]. Indeed, various strategies have been used to organize the semiconductor nanocrystals on substrates. Layer by layer self assembly technique [8], self assembled monolayer (SAMs) technique [8], spin coated charged polymer [9] have been used to produce monolayer or multilayered films of semiconductor nanocrystals [10]. However, the optical properties of the obtained films have not been systematically studied and correlated with the thin film structure. In this work, we vary in a controllable way the affinity of the QDs with the substrate using different SAMs. Our goal is to understand how the self assembly of the QDs on the substrate could influence the optical properties of the film. This work is mandatory to understand the mechanisms controlling the aggregation of nanoparticles in thin films and to correlate the obtained organization of QDs with the measured photoluminescence. To determine how the substrate affinity with the QDs can influence their optical properties, different substrates were realized through surface functionalization using different organo-silanes [11–12]. The optical properties of the obtained QD layers were studied with far field fluorescence spectroscopy and confocal microscopy. The obtained results have been correlated with the structure of the QD layer evidenced by atomic force microscopy.

Materials and methods

Substrates preparation

The process requires high purity of all reagents and extreme cleanliness of the substrates and glassware. The following chemicals were of the highest grade and used as supplied: anhydrous toluene, toluene and ethanol (HPLC grade, ACROS); 3-mercaptopropyltrimethoxysilane (TTS, 95%), 3-aminopropyldimethylethoxysilane (ATS, 97%), undecyltrichlorosilane (ALTS, 97%) (ABCR/Gelest, Karlsruhe, Germany). The substrates and glassware were thoroughly cleaned by immersion into freshly prepared Piranha solution [H_2SO_4, 98%/H_2O_2, 30% 2:1 (v/v)] for at least 30 min, extensively rinsed with deionized water and dried in an oven. The substrates were immersed for 24 h in a 1% solution of silane in anhydrous toluene under argon atmosphere. After washing with a solvent sequence (toluene, ethanol) the substrates were sonicated in toluene, which yielded high-quality silane monolayers. Water contact angles were measured under ambient atmosphere at room temperature by using the sessile drop method and an image analysis of the drop profile with a home made system. Water contact angles were in agreement with expected values [13, 14]. Indeed, we found 106°±0.5, 67°±0.3 and 55°±0.5 for samples ALTS, ATS and TTS, respectively.

Semiconductor nanocrystal deposition

The functionalized substrates were immersed at room temperature for 30 min in a Core shell evidot (CdSe/ZnS/TOPO, Fort orange, Evident Technologies) solutions in toluene with the concentration varying from $2.5 \cdot 10^{-1}$ g/l to $2.5 \cdot 10^{-4}$ g/l. The samples have been subsequently washed under flowing toluene and then dried with argon.

Photoluminescence measurements

Far field photoluminescence spectra have been measured in air at room temperature using a Jobin Yvon (55 cm focal length) spectrometer (spectral resolution<1 nm). Measurements have been performed using two different laser sources without any control of the laser polarization. The first one was the 442 nm ray of a HeCd laser. The second one was a laser diode with an emission wavelength of 405 nm. In both cases the laser beam has been expanded to cover 1 cm^2 on the sample.

Confocal microscopy

The confocal experiments discussed in this paper have been conducted on a home-made fluorescence microscope at room temperature. The setup has been developed from an inverted microscope. Both the excitation at 458 nm (Ar laser) wavelength and the light collection are ensured by a ×60, NA 0.95 dry objective. The sample is placed in a holder driven by a piezoscanner (scan range: 100×100 μm^2). Before reaching the detector, the collected light is filtered by a dichroic mirror at 458 nm that cuts the excitation light. A bandpass filter (542–622 nm) centered on the emission line of the CdSe QDs further narrows the transmission window. The light emitted in the focalization volume of the laser line is then selected by an optical fiber (core diameter: 50 μm) placed in the image plane of the sample. For the detection, we either use a spectrometer equipped with a charge-coupled device (CCD) camera cooled at −110 °C for spectral studies, or an avalanche photodiode (APD) in the photon counting mode for imaging.

Atomic force microscopy

AFM images were recorded in air with a M5 from Park Scientific Instrument using a 100 μm scanner. The images were recorded in intermittent-contact mode (IC-AFM). For IC-AFM, Pointprobe Plus Tapping-mode sensors (PPP-NCLR-20 Nanosensors) were used. These cantilevers had resonance frequency around 146–236 kHz, a typical spring constant of about 21–98 N/m and an integrated Si tip with a radius around 10 nm. A second order flattening (line by line) was performed on AFM images after acquisition.

Results and discussions

Figure 1 shows the photoluminescence spectra measured on different samples obtained by immersion in a $2.5 \cdot 10^{-3}$ g/l QDs solution after functionalization with amine-terminated, alkane-terminated and thiol-terminated silanes. Each spectrum has been obtained for a laser excitation power of 75 mW/cm^2 at 442 nm. Note that the photoluminescence

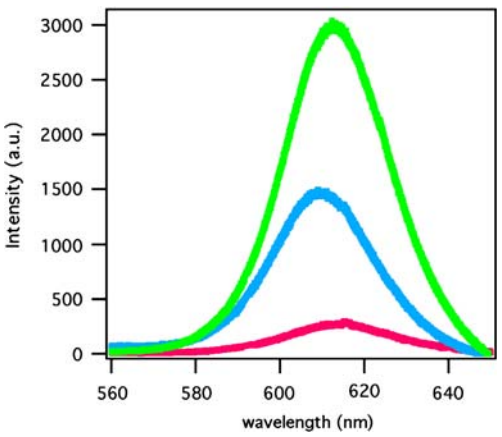

Fig. 1 Photoluminescence spectra of QDs obtained on different substrates: thiol-terminated silane (*green*), amine-terminated silane (*blue*) and alkane-terminated silane (*pink*). Each spectrum has been obtained for a laser excitation power of 75 mW/cm^2 at 442 nm

intensity (PLI) of the QDs varies strongly with the chemical nature of the ligand grafted on the substrate. As shown on the figure, the measured PLI of the QDs on the thiol-terminated silane (TTS) reaches its maximum for a wavelength of about 613±9 nm. The maximum for the QDs on the amine-terminated silane (ATS) is reached at 610±8 nm and at 614±9 nm for the QDs deposited on the alkane-terminated silane (ALTS). Note that the Full Width at Half Maximum of the different spectra (FWHM=26±3 nm) is independent of the chemical nature of the silane and reflects a collective response corresponding to the size distribution of the considered QDs. Second, the measured PLI is higher (3,000 cps) for the QDs deposited on the TTS than for the PLI measured on both the ATS (1,500 cps) and the ALTS (250 cps).

To determine the origin of the large differences in the measured PLI, an AFM study of the different samples has been performed. The AFM images, shown Fig. 2, reveal a significant difference in the structure of the QDs layer depending on the different silanes. Indeed, the film obtained on the thiol-terminated silane is homogeneous showing a disperse monolayer of QDs on the substrate (Fig. 2a). Moreover the profile clearly shows that the monolayer is composed of very small 2D aggregates or single QD. On the other hand, the QD film obtained on the amine-terminated substrate is characterized by larger 3D aggregates (see Fig. 2b) but the thickness varies from the mono to the bilayer as revealed by the profile. Finally, the alkane-silane functionalized substrate shows the less homogeneous QD dispersion (see Fig. 2c). Indeed, the substrate is not well covered and large 3D aggregates are visible. Moreover roughness (rms) measurements reveal that the roughness is about 2.9 nm for the TTS sample, 4.6 nm for the ATS sample and 10 nm for the ALTS sample in good agreement with the observations.

To better understand the behavior observed on our QDs layer, confocal microscopy coupled with single QD (or small aggregate) spectroscopy have been performed. Typical confocal images (10 μm×10 μm) for the concentration of $2.5\cdot10^{-3}$ g/l are shown on Fig. 3. Note that the excitation power is about 90 nW for the TTS and the ATS samples but is about 1,100 nW for the ALTS sample. The normalized mean intensity of each pixel is about 273.35 cps/nW, 37.24 cps/nW and 2.63 cps/nW for the TTS, the ATS and the ALTS, respectively. These results confirm the dependency of the photoluminescence intensities determined above with the surface modification. Moreover, the standard deviation values are σ_{TTS}=104.4 cps/nW, σ_{ATS}=5.75 cps/nW and σ_{ALTS}=2.15 cps/nW, indicating that the QDs distribution is more homogeneous for the TTS and ATS samples than for the ALTS sample.

To determine if the measured differences are coming from an intrinsic change of the individual QD properties or from a change of the collective properties of the QD assembly, single QD spectroscopy has been performed. Typical results are shown Fig. 4 for the different substrates. Thus, for all the functionalized substrates an identical response of an individual QD (or small aggregate) has been found. Indeed, emission wavelengths varying from 590 nm to 610 nm have been measured which correspond to the given size dispersion of the commercial solution. Furthermore, PLI varies from 5 cps to 20 cps indicating a single emitter or a reduced number of emitters (lower than 5) [15, 16]. These results do not show any evidences for the well-known quench induced by the non-protonated amines. This is certainly due to various parameters: first, the core–shell QDs are well stabilized and second, the most important, is that in our experimental conditions (in room temperature in air), amines of the ATS are protonated [12].

Finally, a systematic study of the far field photoluminescence of the most promising samples (TTS) as a function of the laser excitation power at 405 nm has been performed. For this purpose, the concentration of the QD solutions has been varied by four orders of magnitude starting from $2.5\cdot10^{-1}$ g/l to $2.5\cdot10^{-4}$ g/l. Results are shown Fig. 5. Figure 5a shows a

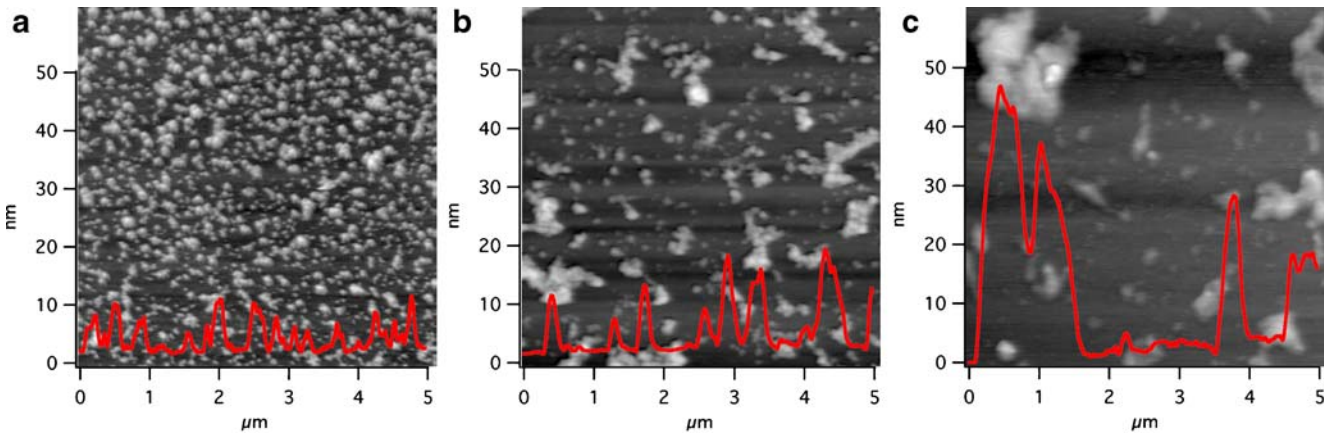

Fig. 2 Typical atomic force microscopy images (Tapping-mode AFM, 5 μm×5 μm) and their associated profiles of the QDs layer obtained on: **a** thiol-terminated silane, **b** amine-terminated silane and **c** alkane-terminated silane

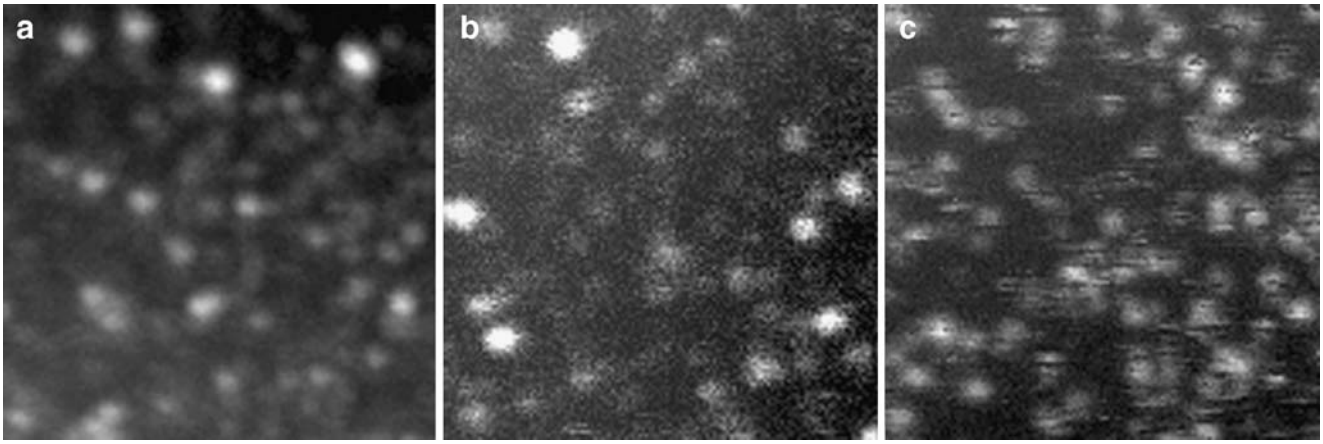

Fig. 3 Typical confocal images (10 μm×10 μm) of the QDs layer obtained on: **a** thiol-terminated silane for an excitation power of 90 nW, **b** amine-terminated silane for an excitation power of 90 nW and **c** alkane-terminated silane for an excitation power of 1,100 nW

typical set of measured spectra for the sample realized using the $2.5 \cdot 10^{-3}$ g/l solution. The laser excitation power varies from 0.1 mW (lower red curve) to 25 mW (higher orange curve). The maximum wavelengths do not vary with the excitation power. Each curve has been integrated in order to obtain the PLI, which is shown on Fig. 5b for all the samples. The PLI increases with the laser excitation power for all the QD concentrations. The PLI increases with the concentration of about one order of magnitude between each concentration indicating a quasi-constant dependence of the PLI with the laser excitation power as clearly evidenced on Fig. 5c. Indeed, Fig. 5c shows the normalized PLI (I/I_{25mW}) for all the different samples. It appears that the PLI dependency is the same (variations are lower than 10%) for all the samples indicating that there are no drastic changes of the photoluminescence induced by the concentration of the

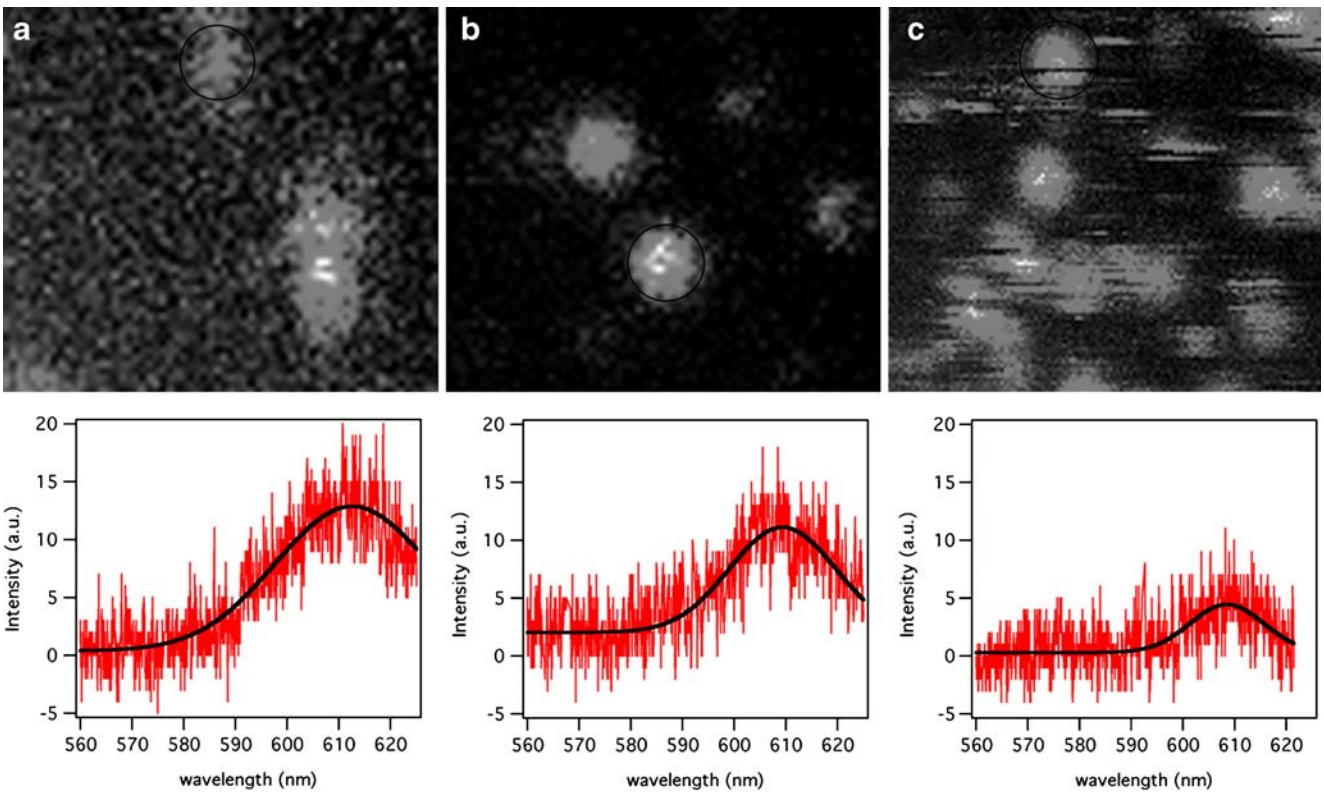

Fig. 4 Confocal images (2 μm×2 μm) and the corresponding spectrum of an isolated QD deposited on: **a** thiol-terminated silane for an excitation power of 90 nW, **b** amine-terminated silane for an excitation power of 90 nW and **c** alkane-terminated silane for an excitation power of 1,100 nW

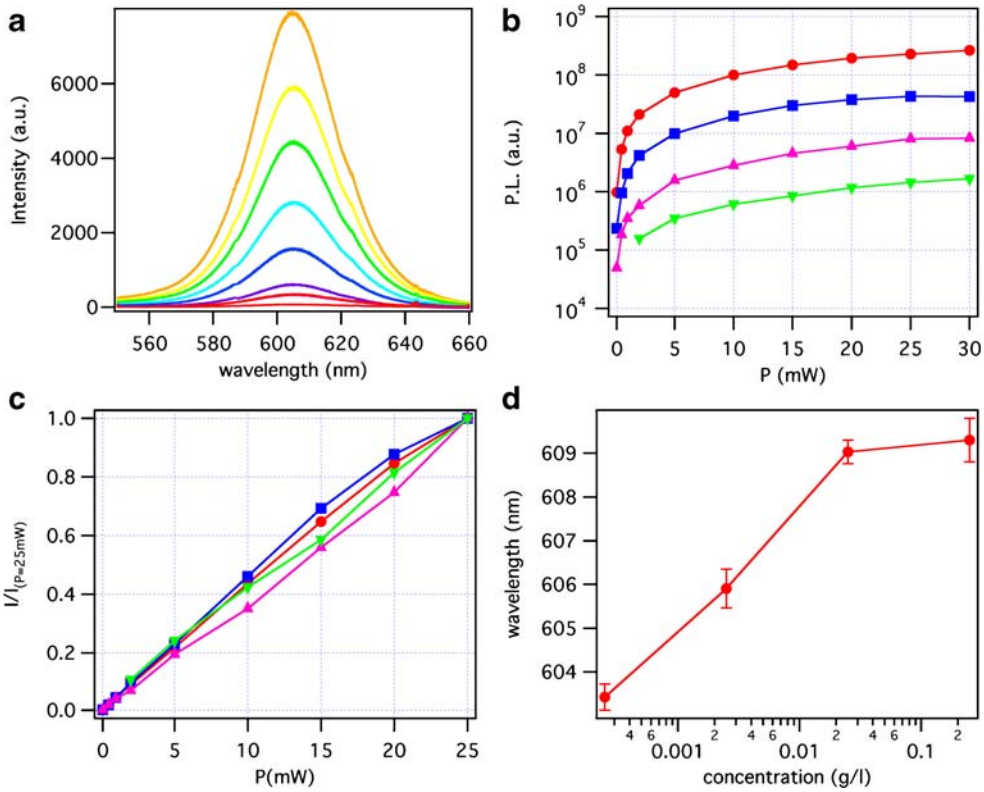

Fig. 5 Photoluminescence measurements obtained on TTS for different QD concentrations. **a** Examples of photoluminescence spectra measured for the TTS sample with [QD]=$2.5\cdot10^{-3}$ g/l as a function of the laser power. **b** Photoluminescence intensity (PLI) vs. laser power measured on the different TTS samples with [QD]=$2.5\cdot10^{-4}$ g/l (▼), $2.5\cdot10^{-3}$ g/l (▲), $2.5\cdot10^{-2}$ g/l (■), $2.5\cdot10^{-1}$ g/l (●). **c** Normalized PLI ($I/_{IP=25mW}$) vs. laser power measured on the different TTS samples with [QD]=$2.5\cdot10^{-4}$ g/l (▼), $2.5\cdot10^{-3}$ g/l (▲), $2.5\cdot10^{-2}$ g/l (■), $2.5\cdot10^{-1}$ g/l (●). **d** Wavelengths corresponding to the maximum of the photoluminescence spectra as a function of the concentration of the QDs

QDs (i.e. no quenching by concentration). On the other hand, the wavelength corresponding to the maximum of the photoluminescence spectra varies with the concentration of the QDs solution as shown Fig. 5d. The maximum wavelength rapidly increases up to 609 nm and then saturates. This red shift could be explained by energy transfer from the blue emitting particles to the red emitting particles arising from dipolar coupling between proximal QDs [17, 18]. Indeed, the 6 nm redshift is in good agreement with the particles size dispersion of about ±5% (i.e. the core diameter varies from 2.75 nm to 3.05 nm) [19]. As shown in Fig. 5, for a high photon absorption probability, the emissive recombination process is higher in the case of the low density layer. Indeed, as shown in Fig. 5d, the non emissive recombination induces a red-shift of the QD emission. Note that this lower emissive recombination in the case of the denser layers do not induce any saturation of the photoluminescence due to the quite low incident beam power used in this study.

The strong difference in photoluminescence efficiency and in structure of our luminescent nanostructures can be explained considering the competition between the different chemical QD–QD and QD–surface interactions [20, 21]. Indeed, the QD–QD interactions are governed by van der Waals interactions between alkane chains of the ligands (TOPO). On the other hand interactions between the QDs and the functionalized substrates are strongly dependent on specific interactions between the QD and the terminal chemical group of silanes (i.e. methyl, amine and thiol). In the case of ALTS, the QD–surface interactions are van der Waals type. From our AFM image (see Fig. 2c), it seems that the energetically more favourable situation is the clustering of QDs in 3D aggregates instead of the organisation in a homogeneous film. This resulting structure could be explained by the difference of density of alkane chains on the surface and on the QDs. Indeed, the high density of the ALTS film, as indicated by the water contact angle, does not allow a strong interdigitation of the chains contrarily to the TOPO layer on the QDs. In the case of ATS, the QD–surface interaction seems better than in the previous case. Indeed, the interactions are certainly governed by long range electrostatic interactions between the protonated amine of the ATS and the slightly negatively charged QDs. Nevertheless the surface coverage remains low and the 3D growth of the clusters is not annihilated. In the last case, the possibility of a pseudo-covalent bond between the TTS and the ZnS shell of the QD induces large forces. Then, the film is completely 2D with a cluster growth parallel to the surface as shown Fig. 2a. As a consequence of these observed structures, the difference in the measured photoluminescence between the different samples could be easily understood. The number of absorbed photons by QD strongly depends on the surface coverage. Indeed, the probability for the photon absorption by a QD is higher in the case of a 2D layer perpendicular to the incident beam than in the other case. This value is maximized in the case of the TTS samples, which shows the strongest photoluminescence.

Moreover this explanation is coherent with the fact that the single emitter shows a photoluminescence very similar [15] (see Fig. 4) indicating that there is no intrinsic change in the QDs (for example, there is no quench induced by the non-protonated amine).

Conclusion

To summarize, the self organization of the QDs on the substrate can be understood considering the affinity of the nanoparticles with the different substrates. It appears clearly from our results that the interaction between the substrate and the nanoparticles must be stronger than the nanoparticle–nanoparticle interaction to avoid 3D aggregation. Furthermore, emission properties of QDs can be at least in a first approximation understood in terms of particles organization rather than intrinsic changes induced by pure surface chemistry.

Acknowledgements We thank support from the "Action Concertée Nanosciences 2004" (NANOPTIP project) and the European Social funds FEDER.

References

1. Park JH, Kim JY, Chin BD, Kim YC, Kim JK, Park OO (2004) White emission from polymer/quantum dot ternary nanocomposites by incomplete energy transfer. Nanotechnology 15:1217–1220, doi:10.1088/0957-4484/15/9/018
2. Nozik AJ (2002) Quantum dot solar cells. Physica E 14:115–120, doi:10.1016/S1386-9477(02)00374-0
3. Grätzel M (2005) Solar energy conversion by dye-sensitized photovoltaic cells. Inorg Chem 44:6841–6851, doi:10.1021/ic0508371
4. Chan WCW, Nie S (1998) Quantum dot bioconjugates for ultrasensitive nonisotopic detection. Science 281:2016–2018, doi:10.1126/science.281.5385.2016
5. Wu X, Liu H, Liu J, Haley KN, Treadway JA, Larson JP et al (2003) Immunofluorescent labeling of cancer marker Her2 and other cellular targets with semiconductor quantum dots. Nat Biotechnol 21:41–46, doi:10.1038/nbt764
6. Sukhanova A, Devy J, Venteo L, Kaplan H, Artemyev M, Oleinikov V et al (2004) Biocompatible fluorescent nanocrystals for immunolabeling of membrane proteins and cells. Anal Biochem 324:60–67, doi:10.1016/j.ab.2003.09.031
7. Klimov VI (2004) Semiconductor and metal nanocrystals. Marcel Dekker, New York
8. Tang Z, Wang Y, Kotov NA (2002) Semiconductor nanoparticles on solid substrates: film structure, intermolecular interactions, and polyelectrolyte effects. Langmuir 18:7035–7040, doi:10.1021/la025601d
9. Huynh WU, Dittmer JJ, Alivisatos AP (2002) Hybrid nanorod-polymer solar cells. Science 295:2425–2427, doi:10.1126/science.1069156
10. Pacifico J, Jasieniak J, Górnez DE, Mulvaney P (2006) Tunable 3D arrays of quantum dots: synthesis and luminescence properties. Small 2:199–203, doi:10.1002/smll.200500226
11. Plain J, Pallandre A, Nysten B, Jonas AM (2006) Nanotemplated crystallization of organic molecules. Small 2:892–897, doi:10.1002/smll.200600059
12. Boutin C, Jaffiol R, Plain J, Royer P (2008) Surface modified single molecules free-diffusion evidenced by fluorescence correlation spectroscopy. J Fluoresc. doi:10.1007/s10895-008-0361-y
13. Pallandre A, Glinel K, Jonas AM, Nysten B (2004) Binary nanopatterned surfaces prepared from alkylsilane monolayers. Nano Lett 4:365–371, doi:10.1021/nl035045n
14. Eigler FS, Georger J, Bhatia SK, Calvert J, Shriver-Lake LC, Bredehorst R (1991) Immobilization of active agents on substrates with a silane and heterobifunctional crosslinking agent. United States Patent 5077210
15. Chevalier N, Nasse MJ, Woehl JC, Reiss P, Bleuse J, Chandezon F et al (2005) CdSe-single-nanoparticle based active tips for near-field optical microscopy. Nanotechnology 16:613–618, doi:10.1088/0957-4484/16/4/047
16. Sonnefraud Y, Chevalier N, Motte J-F, Huant S, Reiss P, Bleuse J et al (2006) Near-field optical imaging with a CdSe single-nanocrystal based active tip. Opt Express 14:10596–10602, doi:10.1364/OE.14.010596
17. Kagan CR, Murray CB, Nirmal M, Bawendi MG (1996) Electronic energy transfer in CdSe quantum dot solids. Phys Rev Lett 76:1517–1520, doi:10.1103/PhysRevLett.76.1517
18. Kagan CR, Murray CB, Bawendi MG (1996) Long-range resonance transfer of electronic excitations in close-packed CdSe quantum-dot solids. Phys Rev B 54:8633–8643, doi:10.1103/PhysRevB.54.8633
19. Franzl T, Shovel A, Rogach AL, Gaponik N, Klar TA, Eychmüller A et al (2005) High-rate unidirectional energy transfer in directly assembled CdTe nanocrystal bilayers. Small 1:392–395, doi:10.1002/smll.200400074
20. Israelachvili JN (1991) Intermolecular and surface forces, 2nd edn. Academic Press, New York
21. Butt HJ, Graf K, Kappl M (2003) Physics and chemistry of interfaces. Wiley-VCH, Weinheim